

PM J03338+3320: Long-Period Superhumps in Growing Phase Following a Separate Precursor Outburst

Taichi KATO,^{1*} Enrique de MIGUEL,^{2,3} William STEIN,⁴ Yutaka MAEDA,⁵
Colin LITTLEFIELD,⁶ Seiichiro KIYOTA,⁷ Tonny VANMUNSTER,⁸
Shawn DVORAK,⁹ Sergey Yu. SHUGAROV,^{10,11} Eugenia S. KALINICHEVA,¹²
Roger D. PICKARD,^{13,14} Kiyoshi KASAI,¹⁵ Lewis M. COOK,¹⁶ Hiroshi ITOH,¹⁷
Eddy MUYLLAERT,¹⁸

¹ Department of Astronomy, Kyoto University, Kyoto 606-8502, Japan

² Departamento de Física Aplicada, Facultad de Ciencias Experimentales, Universidad de Huelva, 21071 Huelva, Spain

³ Center for Backyard Astrophysics, Observatorio del CIECEM, Parque Dunar, Matalascañas, 21760 Almonte, Huelva, Spain

⁴ Center for Backyard Astrophysics, 6025 Calle Paraiso, Las Cruces, New Mexico 88012, USA

⁵ Kaminishiyamamachi 12-14, Nagasaki, Nagasaki 850-0006, Japan

⁶ Department of Physics, University of Notre Dame, 225 Nieuwland Science Hall, Notre Dame, Indiana 46556, USA

⁷ Variable Star Observers League in Japan (VSOLJ), 7-1 Kitahatsutomi, Kamagaya, Chiba 273-0126, Japan

⁸ Center for Backyard Astrophysics Belgium, Walhostraat 1A, B-3401 Landen, Belgium

⁹ Rolling Hills Observatory, 1643 Nightfall Drive, Clermont, Florida 34711, USA

¹⁰ Sternberg Astronomical Institute, Lomonosov Moscow State University, Universitetsky Ave., 13, Moscow 119992, Russia

¹¹ Astronomical Institute of the Slovak Academy of Sciences, 05960 Tatranska Lomnica, Slovakia

¹² Faculty of Physics, Lomonosov Moscow State University, Leninskie gory, Moscow 119991, Russia

¹³ The British Astronomical Association, Variable Star Section (BAA VSS), Burlington House, Piccadilly, London, W1J 0DU, UK

¹⁴ 3 The Birches, Shobdon, Leominster, Herefordshire, HR6 9NG, UK

¹⁵ Baselstrasse 133D, CH-4132 Muttenz, Switzerland

¹⁶ Center for Backyard Astrophysics Concord, 1730 Helix Ct. Concord, California 94518, USA

¹⁷ VSOLJ, 1001-105 Nishiterakata, Hachioji, Tokyo 192-0153, Japan

¹⁸ Vereniging Voor Sterrenkunde (VVS), Moffelstraat 13 3370 Boutersem, Belgium

*E-mail: *tkato@kustastro.kyoto-u.ac.jp

Received 201 0; Accepted 201 0

Abstract

We observed the first-ever recorded outburst of PM J03338+3320, the cataclysmic variable selected by proper-motion survey. The outburst was composed of a precursor and the main superoutburst. The precursor outburst occurred at least 5 d before the maximum of the main

superoutburst. Despite this separation, long-period superhumps were continuously seen between the precursor and main superoutburst. The period of these superhumps is longer than the orbital period by 6.0(1)% and can be interpreted to reflect the dynamical precession rate at the 3:1 resonance for a mass ratio of 0.172(4). These superhumps smoothly evolved into those in the main superoutburst. These observations provide the clearest evidence that the 3:1 resonance is triggered by the precursor outburst, even if it is well separated, and the resonance eventually causes the main superoutburst as predicted by the thermal-tidal instability model. The presence of superhumps well before the superoutburst cannot be explained by alternative models (the enhanced mass-transfer model and the pure thermal instability model) and the present observations give a clear support to the thermal-tidal instability model.

Key words: accretion, accretion disks — stars: novae, cataclysmic variables — stars: dwarf novae — stars: individual (PM J03338+3320)

1 Introduction

Cataclysmic variables (CVs) are composed of a white dwarf and a mass-transferring red (or brown) dwarf filling the Roche lobe. The transferred matter forms an accretion disk. Dwarf novae are a class of CVs characterized by outbursts. SU UMa-type dwarf novae are a subclass of dwarf novae characterized by the presence of superhumps and superoutbursts. Superoutbursts are ~ 0.5 – 1.0 mag brighter than normal outbursts and are accompanied by superhumps, which have periods (superhump periods: P_{SH}) a few percent longer than the orbital period (P_{orb}) [for general information of CVs, DNe, SU UMa-type dwarf novae and superhumps, see e.g. Warner (1995); Hellier (2001)].

Although there had been a long debate regarding the origin of superoutbursts and superhumps, it is now widely believed that superhumps are a result of the eccentric (or flexing) deformation of the accretion disk caused by the 3:1 resonance (Whitehurst 1988; Hirose, Osaki 1990; Lubow 1991a; Lubow 1991b). Osaki (1989) proposed a model [thermal-tidal instability (TTI) model] to explain the occurrence of a superoutburst after a sequence of normal outbursts when the disk radius reaches the 3:1 resonance. Osaki, Meyer (2003) refined this TTI model to explain various types of superoutbursts. In some systems [usually with lower mass-transfer rates (\dot{M})], the mass stored in the disk is sufficient to trigger a superoutburst without experiencing normal outbursts. The extreme cases are WZ Sge-type dwarf novae (see Kato (2015) for a modern review). This TTI model predicted the systematic variation of the disk radius over successive outbursts and superoutbursts. This prediction was finally confirmed in Kepler observations, which led to the strongest ever support to the TTI model (Osaki, Kato 2013a).

On the other hand, it has been demonstrated that periods of superhumps systematically vary (Kato et al. 2009): stage A superhumps (long, constant superhump period), stage B superhumps (short superhump period with systematic period variations) and stage C superhumps (constant period shorter than those of stage B superhumps typically by 0.5%). The super-

hump period reflects the precession rate of the eccentric disk, which is mainly a combination of prograde dynamical precession by the gravitational field of the secondary and the retrograde precession by the pressure gradient in the disk (e.g. Lubow 1992). It has been proposed that stage A superhumps corresponds to the growing phase of the 3:1 resonance (Osaki, Kato 2013b; Kato, Osaki 2013) and the superhump period in this stage reflects the dynamical precession rate at the 3:1 resonance. This expectation was successfully used to determine mass-ratios (q) in many systems (Kato, Osaki 2013).

In the standard TTI model, superoutbursts are triggered by a normal outburst during which the disk radius reaches that of the 3:1 resonance. In actual SU UMa-type dwarf novae, there is diversity how superoutbursts start (cf. Marino, Walker 1979). In some cases, there are superoutbursts preceded by widely separated precursor outbursts. Although the TTI model predicts that the 3:1 resonance (and resultant superhumps) starts to grow during the preceding precursor or sometime after the precursor, observational clues for this interpretation have been limited since it is difficult to make high-quality time-resolved photometry *before* superoutbursts start. The only exception has been continuous observations by the Kepler satellite (Borucki et al. 2010; Koch et al. 2010). Kepler recorded a deep dip between the precursor outburst and main superoutburst in V1504 Cyg. Although a frequency analysis by Osaki, Kato (2014) strongly favored the interpretation by the TTI model, the case of V1504 Cyg was not ideal in that the precursor outburst was not sufficiently separated and that the superhump signal was not continuously present. Here we report an ideal case to test this interpretation: the 2015 superoutburst of PM J03338+3320.

2 PM J03338+3320

PM J03338+3320 is a CV selected by its high proper motion (Skinner et al. 2014).¹ Skinner et al. (2014) indicated that PM J03338+3320 has doubly peaked emission lines of hydrogen and HeI superimposed on a blue continuum. The spectrum was typical for a dwarf nova in quiescence. Skinner et al. (2014) also obtained an orbital period of 0.06663(7) d by a radial-velocity study. The period was suggestive of an SU UMA-type dwarf nova.

On 2015 November 28, E. Muylaert detected the first-ever outburst at an unfiltered CCD magnitude of 14.58 (cvnet-outburst 6781). Although subsequent observations detected superhump-like modulations (vsnet-alert 19303), the object rapidly faded. Although there was some suspicion of a normal outburst, the long period compared to the known orbital period strongly suggested that these modulations were superhumps. The object stayed around 17 mag for three nights and it continuously showed these long-period superhumps (vsnet-alert 19310). The object eventually entered the main superoutburst on December 2–3.

3 Observation and Analysis

The data were obtained under campaigns led by the VSNET Collaboration (Kato et al. 2004). We also used the public data from the AAVSO International Database².

Time-resolved observations were performed in 15 different locations by using 30cm-class telescopes (supplementary table 1). The data analysis was performed just in the same way described in Kato et al. (2009) and Kato et al. (2014) and we mainly used R software³ for data analysis. In de-trending the data, we divided the data into four segments in relation to the outburst phase and used locally-weighted polynomial regression (LOWESS: Cleveland 1979). The times of superhumps maxima were determined by the template fitting method as described in Kato et al. (2009). The times of all observations are expressed in barycentric Julian Days (BJD).

We used phase dispersion minimization (PDM; Stellingwerf 1978) for period analysis and 1σ errors for the PDM analysis was estimated by the methods of Fernie (1989) and Kato et al. (2010).

¹ Although the name PM J03338+3320 was used in Skinner et al. (2014), we use the name used in SIMBAD, conforming the nomenclature convention of the International Astronomical Union. The acronym LSPM was also used in Skinner et al. (2011) and the name LSPM J03338+3320 was used in VSNET reports.

² <<http://www.aavso.org/data-download>>.

³ The R Foundation for Statistical Computing:
<<http://cran.r-project.org/>>.

4 Results

4.1 Outburst Light Curve

As shown in the upper panel of figure 1, this object showed a separate precursor outburst which occurred at least 5 d before the peak of the main superoutburst. The main superoutburst lasted for ~ 7 d. Between the precursor and main superoutburst, the object stayed at ~ 16.8 , ~ 0.5 mag brighter than in quiescence. There was at least one post-superoutburst rebrightening on BJD 2457374–2457375, 7 d after the rapid fading. The object was also caught during the fading part of another outburst on BJD 2457400 (E. de Miguel). It was not certain whether this outburst was the second rebrightening or the first normal outburst of the next supercycle.

4.2 Superhumps

Superhumps were continuously detected already during the fading branch of the precursor outburst (figure 2). The superhumps before the rise to the main superoutburst had a long period [0.07066(1) d in average; figure 3; supplementary table 2]. As shown in the $O - C$ diagram in figure 1, these superhumps showed no period variation. These superhumps smoothly evolved into superhumps during the main superoutburst. The period became slightly shorter when the object approached the maximum of the superoutburst (around $E=60-65$ in figure 1). Superhumps following this phase had a shorter, relatively constant period of 0.06902(2) d between $E=70$ and $E=115$ in figure 1. The period then shortened to another constant one at 0.06876(3) d (figure 4, mean profile after $E=70$; supplementary table 3). These superhumps persisted at least before the rebrightening. We identified these three stages as stage A, B and C as introduced in Kato et al. (2009). The most striking feature is the continuous presence of stage A superhumps between the separate precursor and the main superoutburst. The apparent lack of a phase jump in stage C superhumps when the superoutburst terminated is also worth mentioning.

There is likely modulations of the superhump amplitudes with a period of ~ 30 cycles (see lower panel of figure 1). This is most likely a beat phenomenon between the orbital period and superhump period (the expected beat period is $2.15 \text{ d} = 31$ cycles). The presence of the beat phenomenon is also consistent with the likely high inclination inferred from doubly peaked emission lines in spectroscopy.

5 Discussion

5.1 Separate precursor and stage A superhumps

It has been known that there is a continuous sequence of precursor-main superoutburst in VW Hyi (Marino, Walker 1979). As discussed in subsection 2.2 in Osaki, Kato (2014),

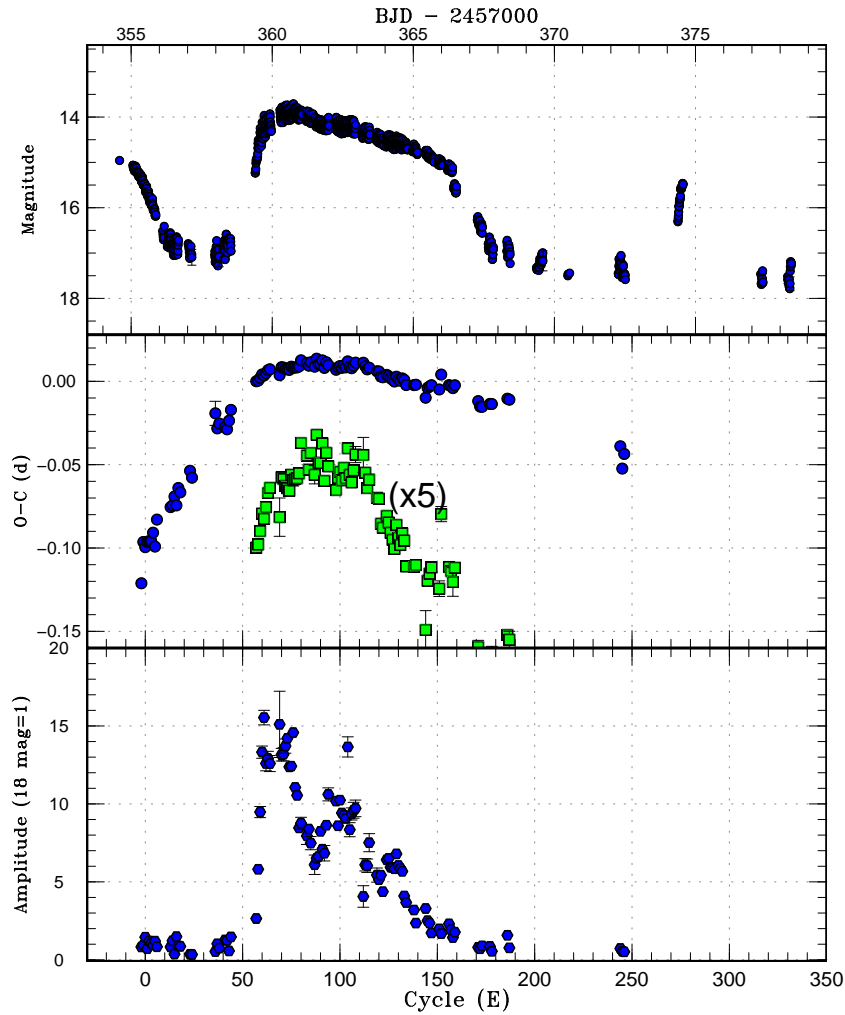


Fig. 1. $O - C$ diagram of superhumps in PM J03338+3320 (2015). (Upper:) Light curve. The data were binned to 0.0069 d. There was at least one post-superoutburst rebrightening on BJD 2457374–2457375. (Middle:) $O - C$ diagram (filled circles). We used a period of 0.0699 d for calculating the $O - C$ residuals. Filled squares are enlarged by five times in the $O - C$ values and shifted arbitrarily to better visualize the stage transitions. (Lower:) Amplitudes of superhumps. The scale is linear and the pulsed flux is shown in a unit corresponding to 18 mag = 1.

this phenomenon can be understood in the framework of the TTI model that the 3:1 resonance is reached during the precursor outburst and superhumps start to grow, finally triggering the main superoutburst. In the case of Kepler data in V1504 Cyg, a frequency analysis has shown that long-period growing superhumps (stage A superhumps) were indeed present between the precursor outburst and main superoutburst (Osaki, Kato 2014). In the case of V1504 Cyg, however, the superhump waves was rather irregular in shape and the signal almost disappeared during the rising branch to the main superoutburst [see figure 5 in Osaki, Kato (2014)]. This made it impossible to make an $O - C$ analysis to see whether the superhumps between the precursor outburst and main superoutburst have the continuous properties as those recorded during the main superoutburst.

The present case of PM J03338+3320 provides an ideal opportunity in studying the properties of the superhumps between the precursor outburst and main superoutburst: the su-

perhump signals were strong and regular and we could measure individual maxima. The result (middle panel of figure 1) clearly indicates that superhumps had the same period and the phase since the precursor until the peak of the main superoutburst. We can now safely say that stage A superhumps were persistently present following the precursor outburst and they smoothly evolved into stage A superhumps during the main superoutburst. The present case is more extreme than in V1504 Cyg in that the precursor is more isolated from the main superoutburst. This finding gives a strong support to the TTI model.

The striking finding is the constancy of the period during and after the precursor outburst despite that the system brightness greatly decreased. As discussed in Kato, Osaki (2013), the fractional superhump excess in frequency $\epsilon^* = 1 - P_{\text{orb}}/P_{\text{SH}}$ has a functional form of $\epsilon^* = Q(q)R(r)$, where r is the disk radius, when the pressure effect can be neglected. When the system is faint (as in the faint state between the precursor outburst

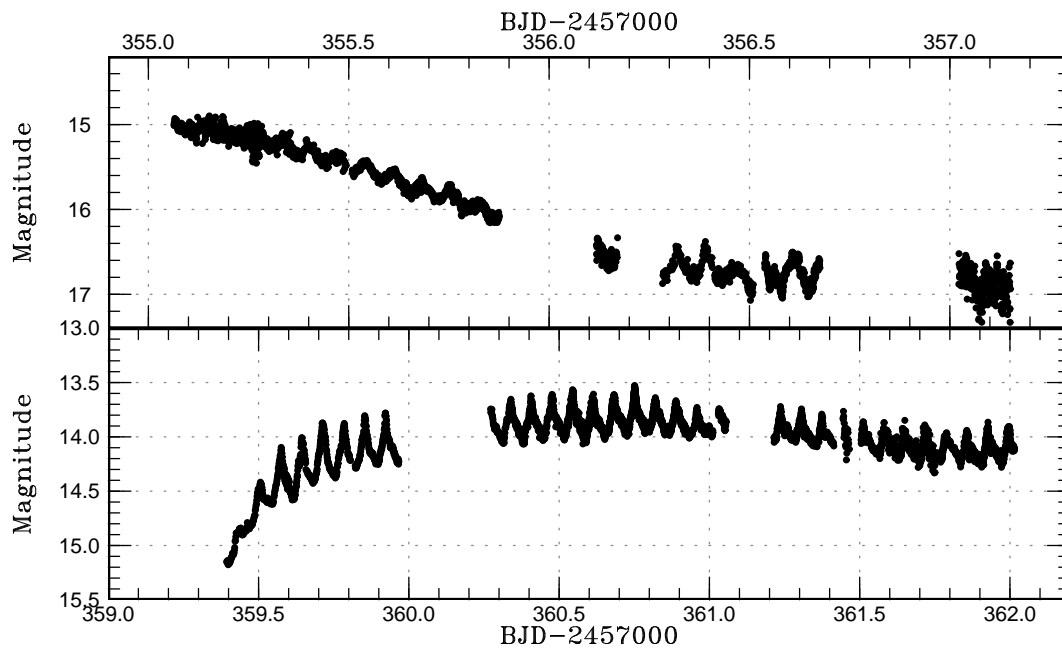


Fig. 2. Superhumps in PM J03338+3320 (2015). (Upper) Fading part of the precursor. (Lower) Initial part of the main superoutburst.

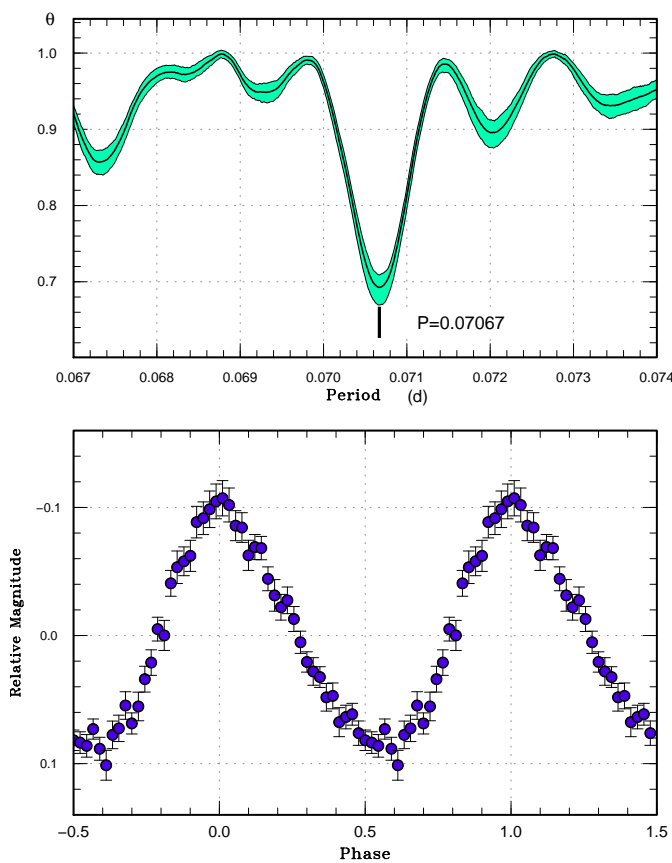


Fig. 3. Superhumps in PM J03338+3320 (2015) from the precursor to the main superoutburst. The data before BJD 2457360 were used. (Upper): PDM analysis. (Lower): Phase-averaged profile.

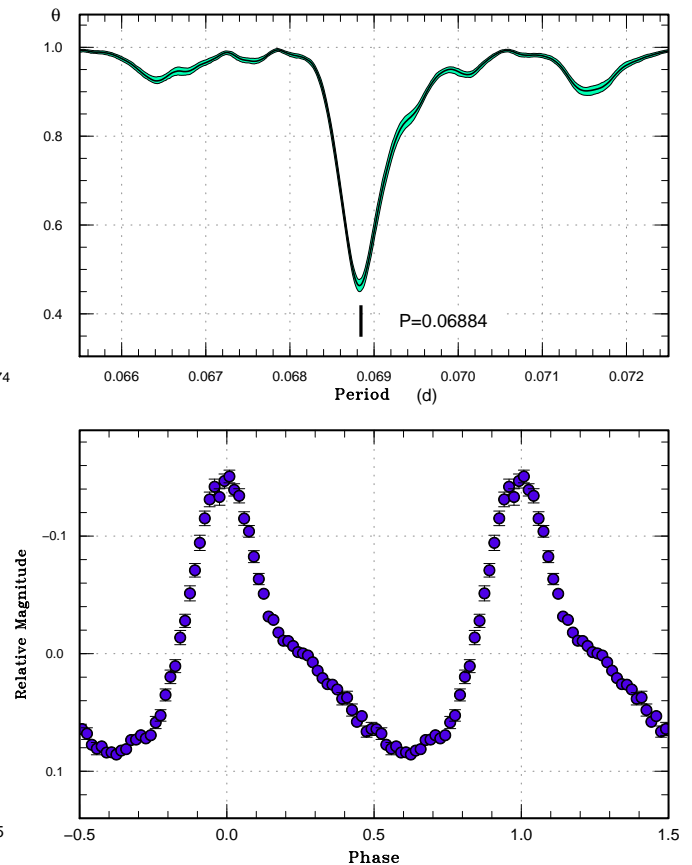


Fig. 4. Superhumps in PM J03338+3320 (2015) during the main superoutburst after transition to stage B superhumps. The data after BJD 2457360 were used. (Upper): PDM analysis. (Lower): Phase-averaged profile.

and main superoutburst), we can safely neglect the pressure effect and the ϵ^* can be used to estimate the change of the radius (cf. Osaki, Kato 2014). The measured ϵ^* for superhumps between the precursor outburst and main superoutburst was large and constant and the disk radius needs to be constant. We consider that this radius represents the radius of the eccentric part of the disk. As shown in subsection 5.2, this radius is compatible with that of the 3:1 resonance assuming a reasonable q for the orbital period. We now have evidence that the eccentric disk at the 3:1 resonance is continuously present between the precursor outburst and main superoutburst, which was supposed, but not sufficiently verified yet, in the TTI model.

5.2 Mass ratio from stage A superhumps

Kato, Osaki (2013) proposed a method to determine q from ϵ^* for stage A superhumps. In the present case, the observed $\epsilon^* = 0.0604(13)$ corresponds to $q=0.172(4)$. This value is somewhat large for a $P_{\text{orb}}=0.06663$ d object (cf. figure 4 in Kato, Osaki (2013)). This large estimated q safely excludes a possibility that the radius where stage A superhumps arose was somewhere inside the 3:1 resonance — if the radius is smaller, it requires an even unlikely larger q for this P_{orb} .

5.3 Difference from V1504 Cyg

In the case of Kepler data of V1504 Cyg, although frequency analysis detected stage A superhumps between the precursor and main superoutburst, individual hump profiles were rather complex and we could not sufficiently measure individual maxima. The profiles in PM J03338+3320, however, were much more clearer and we could measure times of all observed superhumps in the same outburst phase. The difference may be due to the difference in the mass-transfer rate. In the case of V1504 Cyg, the frequent normal outbursts and short supercycle (cf. Osaki, Kato 2013a; Osaki, Kato 2013b; Osaki, Kato 2014) suggests a high mass-transfer rate. In contrast, PM J03338+3320 apparently has much infrequent outbursts. Indeed, no outbursts were recorded in observations on 90 different nights spanning for BJD 2453642–2456593 in the CRTS data (Drake et al. 2009). In the case of V1504 Cyg, the strong mass-accretion flow may have masked low-amplitude stage A superhumps before the main superoutburst by resulting strong flickering. Although the stage A superhump method is expected to work to determine the mass ratio when superhumps start to evolve before the main superoutburst (as in the present case), the best application may be sought for low- \dot{M} objects. This interpretation needs to be confirmed by further observations in different objects.

5.4 Growth time of stage A superhumps

Kato (2015) suggested that the growth time of stage A superhumps in WZ Sge-type dwarf novae can be a good measure of the growth of the 3:1 resonance, which is theoretically expected to be proportional to q^2 (Lubow 1991a; Lubow 1991b). In WZ Sge-type dwarf novae, $q=0.06$ roughly corresponds to the growth time of 60 cycles and the time is usually much shorter in ordinary SU UMa-type dwarf novae. Kato et al. (2016) claimed that in high q systems close to the stability limit of the 3:1 resonance also show slow growth of superhumps, requiring time comparable to WZ Sge-type dwarf novae. The present case of PM J03338+3320 required at least 60 cycles, which is comparable to low- q WZ Sge-type dwarf novae. Since PM J03338+3320 does not have a high q close to the stability limit, this long growth time requires another explanation. The main difference of PM J03338+3320 from WZ Sge-type dwarf novae and other SU UMa-type dwarf novae is the widely separated precursor outburst. Stage A superhumps showed little tendency to grow in amplitude during this phase (lower panel of figure 1), and it is likely that stage A superhumps grow slowly near the quiescent state. Since the growth of stage A superhumps, and finally the spread into the entire disk would require viscous spread of the eccentric region, it may be that the low-viscosity state near quiescence requires more time than in the outbursting disk as in WZ Sge-type dwarf novae and SU UMa-type dwarf novae without separate precursor outbursts. It means that the duration of stage A would not be a good measure of q in systems with separate precursor outbursts. This would, in turn, explain the diversity in the intervals between the precursor outburst and the main superoutburst (cf. ranging from almost continuous transition to intervals as long as 10 d in QZ Vir (1998, Ohshima et al. 2011) and 11 d in V699 Oph (2001, Kato et al. 2009, see Osaki, Kato 2014) since the growth time of stage A superhumps is not a unique function of q near quiescent state.

5.5 Cases of enhanced mass-transfer and pure thermal instability models

Up to this subsection, we considered the TTI model to interpret the observations. As reviewed in Osaki, Kato (2013a), there are currently three models to explain superoutbursts and supercycles. In addition to the TTI model, there are the enhanced mass-transfer (EMT) model advocated by Smak (Smak 1991, Smak 2004, Smak 2008), and the pure thermal instability model by Cannizzo in the original form (Cannizzo et al. 2010, Cannizzo et al. 2012).

In the present case, superhumps appeared well before the main superoutburst, which excludes the EMT model as already discussed in Osaki, Kato (2013a). We consider here if the present observations can be explained by the pure thermal instability model. As reviewed in Osaki, Kato (2013a), this model

claims that normal outbursts and superoutbursts are equivalent to “narrow” and “wide” outbursts seen in SS Cyg-type dwarf novae and that superhumps are excited as the result of the expansion of the disk during wide outbursts. In this model, heating wave from the inner part of the disk is reflected before reaching the outer edge of the disk in normal outbursts [see figures 3, 4 in Cannizzo et al. (2010); this type of outburst corresponds to type ‘Bb’ in the classification by Smak (1984)]. Only in superoutbursts the heating wave reaches the outer edge. In the pure thermal instability model, precursor outbursts (or shoulders) are formed since the speed of the heating wave becomes slower when it passes through the disk mass which has been accumulated during repeated cycles of normal outbursts preceding the superoutburst. During such precursors, the heating wave should not be reflected since such reflection will quench the outburst (see subsection 3.2 in Osaki, Kato 2013a). There should not be a deep dip between the precursor (shoulder) and the peak of the main superoutburst (see also subsection 2.2 in Osaki, Kato 2014). Its natural consequence is that it is impossible to reproduce a separate precursor as seen in the present observations. Another difficulty in the pure thermal instability model is that the disk does not expand during normal outbursts or the precursor (shoulder) phase, since the heating wave does not reach the outer edge of the disk. In this model, the disk cannot reach the 3:1 resonance before the heating wave reaches close to the outer edge, i.e. around the peak of the superoutburst. The presence of long-period superhumps well before the superoutburst, which is the direct consequence of the disk reaching the 3:1 resonance, cannot be explained by the pure thermal instability model and the TTI model is the only model which can explain the present observations.

In this subsection, we used “in the original form” for the pure thermal instability model by Cannizzo. This was because Cannizzo (2015) recently introduced a pure thermal instability model allowing the radius variation of the disk and claimed that this model could reproduce the SU UMa-type supercycle. Although this model appears to have successfully reproduced the presence of a precursor outburst, the reason why such a precursor was made possible is unclear since this paper is a conference proceeding and no details of the model were given. It would be better for a full article on this model to appear to make a fair comparison between the TTI model with this new extension of the pure thermal instability model and we restrict our discussion to the original pure thermal instability model. We can, however, point out that the model in Cannizzo (2015) would predict the constant disk radius during the superoutburst (as in figure 2 in Cannizzo 2015), which contradicts the observation, such as the decrease in the disk radius measured in eclipsing systems (see e.g. figure 10 in Osaki, Kato 2014) and the systematic decrease of the superhump periods (i.e. precession rates) between superhump stages B and C.

6 Summary

We observed the 2015 superoutburst of PM J03338+3320. The superoutburst was preceded by a separate precursor outburst which occurred at least 5 d before the maximum of the main superoutburst. Superhumps were continuously present during the fading branch of the precursor and persisted until the rise to the main superoutburst. The $O - C$ analysis has shown that these superhumps (stage A superhumps) have continuous phases and a constant period all the time before the maximum of the main superoutburst. The period was very long, 0.07066(1) d, 6.0(1)% longer than the orbital period, and can be interpreted to reflect the dynamical precession rate at the 3:1 resonance for a mass ratio of 0.172(4). This result provides the clearest evidence that the 3:1 resonance starts to operate around the precursor outburst, even if it is well separated, and this resonance eventually results the main superoutburst as predicted by the thermal-tidal instability model. These superhumps took long time (more than 60 cycles) to evolve, suggesting that stage A superhumps persist longer time (or take longer time to fully evolve) when the system is near quiescence than in the outburst state. This could explain the wide variety of intervals between the precursor and the main superoutburst. The presence of superhumps well before the superoutburst cannot be explained by alternative models (the enhanced mass-transfer model and the pure thermal instability model) and the present observations give a clear support to the thermal-tidal instability model.

Acknowledgments

This work was supported by the Grant-in-Aid “Initiative for High-Dimensional Data-Driven Science through Deepening of Sparse Modeling” (25120007) from the Ministry of Education, Culture, Sports, Science and Technology (MEXT) of Japan. We acknowledge with thanks the variable star observations from the AAVSO International Database contributed by observers worldwide and used in this research. The authors are grateful to observers of VSNET Collaboration and VSOLJ observers who supplied vital data. We are grateful to the anonymous referee for drawing our attention to the pure thermal instability model and Prof. Yoji Osaki for helpful comments. This work also was partially supported by grants of RFBR 15-32-50920 and 15-02-06178, 14-02-00825 and by the VEGA grant No. 2/0002/13.

Supporting information

Additional supporting information in the online version of this article in PASJ: Tables 1, 2, 3.

Table 1. Log of observations of PM J03338+3320 (2015)

Start*	End*	N^\dagger	Code [‡]	filter [§]	Start*	End*	N^\dagger	Code [‡]	filter [§]
57355.0583	57355.2732	385	Mdy	C	57363.1758	57363.2750	54	Shu	C
57355.1568	57355.3496	215	Ioh	C	57363.2322	57363.3427	149	RAE	V
57355.2755	57355.6777	482	deM	C	57363.2411	57363.4529	281	CDZ	C
57355.5031	57355.8485	390	BJA	C	57363.6883	57363.9489	344	SWI	V
57355.7491	57355.8698	295	COO	C	57364.0347	57364.3080	684	Mdy	C
57356.1126	57356.1654	120	Mdy	C	57364.3162	57364.4267	113	Van	C
57356.2777	57356.5040	221	deM	C	57364.4108	57364.5892	152	Shu	C
57356.5324	57356.6701	376	LCO	C	57364.5434	57364.7917	304	DKS	C
57357.0169	57357.1456	262	Mdy	C	57364.9669	57365.1251	210	Mdy	C
57357.9564	57358.1116	305	Mdy	C	57365.0079	57365.1449	301	Kis	C
57358.2716	57358.5370	147	deM	C	57365.4313	57365.6558	310	RPc	V
57359.3884	57359.5962	166	deM	C	57365.5197	57365.7292	252	DKS	C
57359.5608	57359.9611	500	SWI	V	57365.8744	57366.0356	374	Kis	C
57360.2665	57360.6119	401	deM	C	57366.2104	57366.3845	220	Van	C
57360.3357	57360.6309	244	Shu	C	57366.4192	57366.5233	134	Kai	C
57360.4993	57360.9179	920	BJA	C	57367.2630	57367.4397	210	deM	C
57360.5564	57360.9585	520	SWI	V	57367.6499	57367.8332	224	DKS	C
57360.5627	57360.7461	459	LCO	C	57368.3059	57368.4264	129	RPc	C
57360.7774	57360.9686	104	COO	C	57369.3588	57369.5860	41	Shu	C
57360.9562	57361.0502	178	Kis	C	57370.4704	57370.4794	4	Shu	C
57361.2089	57361.3714	254	Shu	C	57372.2571	57372.5108	210	deM	C
57361.2356	57361.4084	220	Van	C	57374.3709	57374.5600	145	deM	C
57361.3066	57361.4600	40	CDZ	C	57377.3073	57377.3875	65	deM	C
57361.4993	57361.7734	600	BJA	C	57378.2637	57378.3963	111	deM	C
57361.5617	57361.7452	243	CDZ	C	57382.2677	57382.2968	25	deM	C
57361.7101	57361.9306	292	SWI	V	57386.3241	57386.3386	13	deM	C
57361.8531	57362.0093	363	Kis	C	57393.2677	57393.3415	60	deM	C
57362.2419	57362.6629	557	CDZ	C	57400.2860	57400.2922	5	deM	C
57362.3846	57362.6203	236	Van	C	57401.2771	57401.2877	8	deM	C
57362.4499	57362.6643	287	Kai	V	57403.2826	57403.2872	4	deM	C
57362.4824	57362.6720	753	LCO	C	–	–	–	–	–

*JD–2400000.

†Number of observations.

‡Key to observers: COO (L. Cook), DKS (S. Dvorak), deM (E. de Miguel), Ioh (H. Itoh), Kai (K. Kasai), Kis (S. Kiyota), LCO (C. Littlefield), Mdy (Y. Maeda), RPc (R. Pickard), Shu (S. Shugarov team), SWI (W. Stein), Van (T. Vanmunster), BJA, CDZ, RAE (AAVSO observations).

§The filter name C represents unfiltered observations.

Table 2. Superhump maxima of PM J03338+3320 (2015) before the main superoutburst

E	max*	error	$O - C^\dagger$	N^\ddagger
0	57355.2416	0.0028	-0.0164	152
1	57355.3354	0.0014	0.0064	126
2	57355.4013	0.0009	0.0014	63
3	57355.4735	0.0019	0.0027	59
4	57355.5429	0.0003	0.0012	147
5	57355.6120	0.0004	-0.0006	147
6	57355.6860	0.0006	0.0025	106
7	57355.7467	0.0013	-0.0078	116
8	57355.8319	0.0011	0.0065	186
15	57356.3223	0.0007	0.0006	52
16	57356.3923	0.0005	-0.0003	55
17	57356.4667	0.0014	0.0031	57
18	57356.5304	0.0019	-0.0041	66
19	57356.6098	0.0005	0.0044	154
20	57356.6762	0.0009	-0.0001	77
25	57357.0341	0.0033	0.0033	80
26	57357.0990	0.0030	-0.0027	116
38	57357.9656	0.0072	0.0129	45
39	57358.0256	0.0010	0.0020	125
40	57358.0975	0.0014	0.0030	99
43	57358.3023	0.0008	-0.0049	42
44	57358.3700	0.0011	-0.0081	31
45	57358.4442	0.0024	-0.0049	36
46	57358.5197	0.0027	-0.0003	22

*BJD-2400000.

 \dagger Against max = 2457355.2581 + 0.070910*E*. \ddagger Number of points used to determine the maximum.

References

- Borucki, W. J., et al. 2010, *Science*, 327, 977
- Cannizzo, J. K. 2015, *Acta Polytechnica CTU proceedings*, 2, 156
- Cannizzo, J. K., Smale, A. P., Wood, M. A., Still, M. D., & Howell, S. B. 2012, *ApJ*, 747, 117
- Cannizzo, J. K., Still, M. D., Howell, S. B., Wood, M. A., & Smale, A. P. 2010, *ApJ*, 725, 1393
- Cleveland, W. S. 1979, *J. Amer. Statist. Assoc.*, 74, 829
- Drake, A. J., et al. 2009, *ApJ*, 696, 870
- Fernie, J. D. 1989, *PASP*, 101, 225
- Hellier, C. 2001, *Cataclysmic Variable Stars: How and why they vary* (Berlin: Springer)
- Hirose, M., & Osaki, Y. 1990, *PASJ*, 42, 135
- Kato, T. 2015, *PASJ*, 67, 108
- Kato, T., et al. 2014, *PASJ*, 66, 90
- Kato, T., et al. 2009, *PASJ*, 61, S395
- Kato, T., et al. 2010, *PASJ*, 62, 1525
- Kato, T., & Osaki, Y. 2013, *PASJ*, 65, 115
- Kato, T., et al. 2016, *PASJ*, in press (arXiv:1512.05459)
- Kato, T., Uemura, M., Ishioka, R., Nogami, D., Kunjaya, C., Baba, H., & Yamaoka, H. 2004, *PASJ*, 56, S1
- Koch, D. G., et al. 2010, *ApJ*, 713, L79
- Lubow, S. H. 1991a, *ApJ*, 381, 259
- Lubow, S. H. 1991b, *ApJ*, 381, 268
- Lubow, S. H. 1992, *ApJ*, 401, 317
- Marino, B. F., & Walker, W. S. G. 1979, in *IAU Colloq. 46, Changing Trends in Variable Star Research*, ed. F. M. Bateson, J. Smak, & J. H. Urch (Univ. of Waikato, Hamilton, N. Z.), p. 29
- Ohshima, T., et al. 2011, *PASJ*, submitted
- Osaki, Y. 1989, *PASJ*, 41, 1005
- Osaki, Y., & Kato, T. 2013a, *PASJ*, 65, 50
- Osaki, Y., & Kato, T. 2013b, *PASJ*, 65, 95
- Osaki, Y., & Kato, T. 2014, *PASJ*, 66, 15
- Osaki, Y., & Meyer, F. 2003, *A&A*, 401, 325
- Skinner, J. N., Thorstensen, J., & Lépine, S. 2011, in *American Astronomical Society Meeting Abstracts #218 Vol. 43 of Bulletin of the American Astronomical Society* (American Astronomical Society), p. #127.10
- Skinner, J. N., Thorstensen, J. R., & Lépine, S. 2014, *AJ*, 148, 115
- Smak, J. 1984, *Acta Astron.*, 34, 161
- Smak, J. 2004, *Acta Astron.*, 54, 221
- Smak, J. 2008, *Acta Astron.*, 58, 55
- Smak, J. I. 1991, *Acta Astron.*, 41, 269
- Stellingwerf, R. F. 1978, *ApJ*, 224, 953
- Warner, B. 1995, *Cataclysmic Variable Stars* (Cambridge: Cambridge University Press)
- Whitehurst, R. 1988, *MNRAS*, 232, 35

Table 3. Superhump maxima of PM J03338+3320 (2015) during the main superoutburst and post-superoutburst

E	max*	error	$O - C^\dagger$	N^\ddagger	E	max*	error	$O - C^\dagger$	N^\ddagger
0	57359.4339	0.0006	-0.0152	45	55	57363.2400	0.0021	0.0085	85
1	57359.5032	0.0004	-0.0146	42	56	57363.3068	0.0006	0.0066	150
2	57359.5738	0.0003	-0.0127	91	57	57363.3740	0.0007	0.0050	75
3	57359.6449	0.0003	-0.0104	65	58	57363.4440	0.0007	0.0062	56
4	57359.7133	0.0003	-0.0108	72	62	57363.7178	0.0007	0.0050	69
5	57359.7837	0.0003	-0.0092	66	63	57363.7867	0.0004	0.0051	72
6	57359.8544	0.0003	-0.0072	71	64	57363.8527	0.0005	0.0023	73
7	57359.9240	0.0004	-0.0064	73	65	57363.9212	0.0004	0.0021	73
12	57360.2655	0.0023	-0.0088	25	67	57364.0607	0.0004	0.0039	116
13	57360.3393	0.0003	-0.0038	85	68	57364.1289	0.0003	0.0034	138
14	57360.4081	0.0003	-0.0038	117	69	57364.1966	0.0003	0.0024	143
15	57360.4763	0.0003	-0.0043	100	70	57364.2648	0.0003	0.0018	140
16	57360.5450	0.0002	-0.0044	266	71	57364.3327	0.0005	0.0009	67
17	57360.6137	0.0002	-0.0044	418	72	57364.4046	0.0005	0.0040	64
18	57360.6846	0.0002	-0.0023	341	73	57364.4720	0.0004	0.0027	46
19	57360.7529	0.0002	-0.0028	216	74	57364.5402	0.0004	0.0020	71
20	57360.8221	0.0002	-0.0024	224	75	57364.6105	0.0004	0.0037	79
21	57360.8912	0.0002	-0.0021	223	76	57364.6787	0.0005	0.0030	67
22	57360.9608	0.0003	-0.0012	122	77	57364.7446	0.0006	0.0002	66
23	57361.0334	0.0007	0.0026	73	81	57365.0205	0.0006	0.0010	150
26	57361.2389	0.0005	0.0018	117	82	57365.0898	0.0005	0.0015	205
27	57361.3062	0.0003	0.0004	180	87	57365.4270	0.0023	-0.0052	38
28	57361.3772	0.0005	0.0026	102	88	57365.5019	0.0006	0.0010	81
30	57361.5126	0.0011	0.0004	78	89	57365.5717	0.0005	0.0020	145
31	57361.5864	0.0004	0.0054	184	90	57365.6415	0.0006	0.0030	133
32	57361.6520	0.0004	0.0023	193	94	57365.9149	0.0009	0.0014	127
33	57361.7210	0.0004	0.0025	235	95	57365.9929	0.0009	0.0106	128
34	57361.7923	0.0004	0.0051	104	99	57366.2625	0.0006	0.0051	69
35	57361.8569	0.0006	0.0008	134	100	57366.3310	0.0006	0.0048	70
36	57361.9292	0.0004	0.0044	174	101	57366.3987	0.0017	0.0038	34
37	57361.9966	0.0003	0.0030	105	102	57366.4694	0.0005	0.0057	69
41	57362.2698	0.0003	0.0011	67	114	57367.2879	0.0008	-0.0011	53
42	57362.3402	0.0003	0.0028	73	115	57367.3536	0.0009	-0.0041	66
43	57362.4099	0.0002	0.0037	107	116	57367.4225	0.0010	-0.0040	51
44	57362.4779	0.0003	0.0030	265	120	57367.7003	0.0009	-0.0014	67
45	57362.5484	0.0002	0.0047	435	121	57367.7692	0.0018	-0.0012	68
46	57362.6162	0.0002	0.0037	409	129	57368.3244	0.0005	0.0038	50
47	57362.6888	0.0003	0.0075	94	130	57368.3928	0.0010	0.0035	52
48	57362.7546	0.0005	0.0045	72	187	57372.2978	0.0008	-0.0115	46
49	57362.8227	0.0004	0.0038	73	188	57372.3535	0.0015	-0.0246	46
50	57362.8931	0.0005	0.0055	73	189	57372.4312	0.0013	-0.0156	47
51	57362.9640	0.0010	0.0076	24	-	-	-	-	-

*BJD-2400000.

 \dagger Against max = 2457359.4490 + 0.068772*E*. \ddagger Number of points used to determine the maximum.